Optics and Lasers in Engineering 165 (2023) 107541

Contents lists available at ScienceDirect

Optics and Lasers in Engineering

journal homepage: www.elsevier.com/locate/optlaseng

High-speed compressive wide-field fluorescence microscopy with an alternant deep denoisers-based image reconstruction algorithm

Yilin He[a,1], Yunhua Yao[a,1], Yu He[a], Zhengqi Huang[a], Pengpeng Ding[a], Dalong Qi[a], Zhiyong Wang[b], Tianqing Jia[a], Zhenrong Sun[a], Shian Zhang[a,c,d,*]

[a] State Key Laboratory of Precision Spectroscopy, School of Physics and Electronic Science, East China Normal University, Shanghai 200062, China
[b] School of Mathematical Sciences, University of Electronic Science and Technology of China, Chengdu 611731, China
[c] Collaborative Innovation Center of Extreme Optics, Shanxi University, Taiyuan 030006, China
[d] Collaborative Innovation Center of Light Manipulations and Applications, Shandong Normal University, Jinan 250358, China

ARTICLE INFO

Keywords:
Wide-field fluorescence microscopy
High-speed microscopy
Compressive imaging
Image reconstruction
Deep denoisers

ABSTRACT

As an indispensable tool to observe the microcosmic structures and dynamics, wide-field fluorescence microscopy (WFM) has been widely applied in biological and medical areas, but the low imaging speed hinders its applications in high-speed fluorescent dynamics due to the limited frame rate of the camera. Here, we develop a high-speed compressive wide-field fluorescence microscopy (CWFM) to break the imaging speed limitation of conventional WFM. In our CWFM method, a coded aperture temporal compressive imaging technique is introduced into conventional WFM system to accelerate the imaging speed by reconstructing multiple images from every compressed image. An iterative algorithm with alternant deep denoisers of FFDnet and FastDVDnet is designed to reconstruct high-quality sequential images from every compressed image through spatial denoising and temporal constraining. The high-speed imaging ability of CWFM is verified by measuring the movement of fluorescence beads on a slide, and an imaging speed of 2000 Hz is experimentally obtained with an ordinary CMOS camera of 200 Hz, the imaging speed is increased by an order of magnitude. Using our high-speed CWFM system, we successfully observe the hydrodynamics by detecting the flow of fluorescence beads in the water across a corner of microchannel. This technique provides a well-established tool for detecting the high-speed fluid and biological dynamic scene, especially in microflow and cell tracking.

1. Introduction

Wide-field fluorescence microscopy (WFM) [1,2], as a well-established tool to observe the microcosmic structures and dynamics, features with high sensitivity, low background and high specification, which has been widely applied in biological and medical areas, such as cell biology [3,4], immunology [5,6], and clinical pathology [7,8], and so on. Recently, biomedical dynamics has raised strict requirement for obtaining higher imaging speed. However, only the imaging speed with tens to hundreds of frames per second (fps) for existing WFM is available due to the low throughput of ordinary cameras. Urged by the requirement for high-speed WFM, various methods have been developed. On the one hand, a high-speed camera with higher acquirement speed is utilized instead of the ordinary camera in WFM to directly increase the imaging speed. For example, Gelderblom reported a fluorescence imaging of microbubble-induced sonoporation with the frame rate of 1000 Hz utilizing a fluorescence system with the high-speed camera [9]. Sugii et al. measured the velocity distributions of dyed red blood cells and plasma seeded with fluorescent particles with the temporal resolution of 6000 Hz by an epi-microscope equipped with a high-speed camera with an image intensifier [10]. This strategy is easy to be implemented, but there are still some disadvantages, including higher cost and limited recording time of high-speed camera. On the other hand, compressed sensing-based scheme is also introduced into conventional WFM system to increase the imaging speed by exploiting the sparsity of fluorescence images [11]. Generally, compressed sensing-based WFM can be divided into two categories according to the device that is utilized to record the fluorescence signal, one is single pixel camera scheme with a bucket detector [12–14], and the other is compressed camera scheme with a 2D image sensor. The single pixel camera scheme has the advantages of low cost, simple configuration, wide spectral range and high signal-noise-ratio (SNR), but the imaging speed is still limited by the massive coding operation for spatial-temporal modulation, especially for the fluorescence image of large field of view. In contrast,

* Corresponding author.
E-mail address: sazhang@phy.ecnu.edu.cn (S. Zhang).
[1] These authors contributed equally to this work.

https://doi.org/10.1016/j.optlaseng.2023.107541
Received 17 April 2022; Received in revised form 14 January 2023; Accepted 18 February 2023
0143-8166/© 2023 Published by Elsevier Ltd.

the compressed camera scheme is more desirable for higher speed microscopy with simultaneous 2D data acquirement of millions of pixels. For example, Yuan and Pang presented a compressive video microscope based on structured illumination with incoherent light source [15], and demonstrated a temporal compression ratio of 4:1. Qiao et al. developed a snapshot temporal compressive microscopy with the imaging speed of 1000 fps using a reconstruction algorithm of deep image prior [16]. To be more specific, there are two different coding strategies for the temporal compressive WFM with the 2D image sensor, i.e., coding on the illumination pattern and coding on the fluorescence image. The former one has the advantage of less fluorescence photon loss during the imaging collection, and thus the higher SNR can be acquired with the less photobleaching and photodamage on the sample. However, this coding strategy is only suitable for the incoherent illumination source because of the diffraction of coding mask, which means the laser source can't be directly used in this strategy unless being decoherent. Besides, the spatial resolution will also be degraded because of the distortion of coding pattern after passing through the objective lens, and the temporal compressive rate is also comparably lower. As for the coding on the fluorescence image, the collection efficiency of fluorescence signal is reduced by 50% due to the binary spatial coding, but the fine spatial coding can increase the spatial resolution, and the higher temporal compressive rate is available.

Coded aperture temporal compressive imaging has shown to be an effective way to greatly improve the imaging speed with little requirement for hardware updating. To recover the sequential images from every compressed image, various algorithms have been developed [17], including the classical algorithms, such as TwIST [18] and GAP-TV [19] that employ the total variation regularization, BM3D [20] that uses the nonlocal similarity in natural images, GMM [21] that builds up a Gaussian mixture noise model, and DeSCI [22] that utilizes rank minimization. However, due to the low photon number under the short exposure time, it is still a great challenge to fulfill high-quality image reconstruction in the compressed sensing-based WFM. In recent years, some data-driven priors are also adopted in the coded aperture temporal compressive imaging, which show the better performance than the traditional model-based algorithms, such as DnCNN [23], FFDnet [24] and FastDVDnet [25]. However, more ambiguous artifacts and distortions will appear in the reconstructed sequential images compared with the model-based algorithms, which hampers the applications of compressed sensing-based WFM in biomedical imaging.

To overcome the imaging speed limitation of conventional WFM and improve the image reconstruction quality of compressed sensing-based WFM, here we develop a high-speed compressive wide-field fluorescence microscopy (CWFM) with an alternant deep denoisers-based image reconstruction algorithm. In our CWFM system, we utilize the coded aperture temporal compressive imaging with the strategy of coding on the fluorescent image to greatly accelerate the imaging speed, and thus the high spatial resolution and high temporal compressive rate can be achieved. Moreover, to obtain the high-quality sequential images recovered from every compressed image with low SNR under high-speed imaging, an iterative algorithm with alternant deep denoisers is specially designed to overcome the drawbacks of artifacts and distortions in the image reconstruction and keep the advantages of high-fidelity spatial information in deep-learning-based algorithm. The denoising modules of FFDnet and FastDVDnet are alternately utilized in the iterative image reconstruction, which mainly devote to the single frame denoising and temporal coherence maintaining, respectively. Through this special design, high-speed CWFM with few artifacts and flickers is achieved. By imaging the movement of fluorescence beads on a slide, the high-speed imaging ability of CWFM is experimentally confirmed, and an imaging speed of 2000 Hz is obtained with an ordinary CMOS camera of 200 Hz, which is increased by an order of magnitude. Based on our high-speed CWFM system, the hydrodynamics is studied by measuring the flow of fluorescence beads in the water across a corner of microchannel.

2. Experimental design

The experimental arrangement of high-speed CWFM is shown in Fig. 1. A continuous laser with the wavelength of 532 nm is used as the illumination source. The laser is first expanded by a beam expander (BE), then it passes through a lens (L1) and goes through an objective lens (OL) after being reflected by a dichroic mirror (DM), and finally it illuminates on a dynamic sample. The fluorescence signal is collected with the same objective lens and imaged on a digital micromirror device (DMD), which is used to modulate the fluorescence signal with fast-switching binary pseudo random patterns. The coded fluorescence signal is finally accumulated and recorded by a CMOS camera. DMD and CMOS camera are synchronically triggered by a FPGA controller to make sure the fixed coding pattern switching during every exposure of CMOS camera, as shown in the inset of Fig. 1. The video with compressed images is used to recover the dynamic fluorescent scene.

To characterize the spatial resolution of our high-speed CWFM system in static mode, the polystyrene fluorescent beads (Excitation/Emission wavelengths: 540 nm/580 nm) with the diameter of 50 nm are imaged. The diameter of fluorescent beads is smaller than the theoretical spatial resolution limitation, but it can't be similarly treated as point emitters, because the fluorescence distribution inside the bead can't be ignored. Here, the intensity distributions of multiple fluorescent beads are extracted from the collected images, then the average distribution is modified by a model from bead spread function (BSF) to point spread function (PSF) [26], and finally the PSF fitting curve of our CWFM system is obtained, as shown in Fig. 2(a), associated with a measured image of a 50 nm fluorescent bead. The spatial resolution of our CWFM system is determined as 408.9 nm based on the full width at half maximum (FWHM) of PSF. The corresponding modulation transfer function (MTF) is also given in Fig. 2(b). The spatial resolution is slightly worse than the optical diffraction limitation, which should mainly result from the compressed temporal imaging system after the microscope.

The image acquirement in the high-speed CWFM system can be modeled by the following process. The fluorescent dynamics $\{X_i\}_{i=1}^{k} \in R^{n_x \times n_y}$ is modulated by a series of coding patterns, i.e.,$\{C_i\}_{i=1}^{k} \in R^{n_x \times n_y}$, and then the modulated fluorescent dynamics is accumulated into a single image, i.e., $Y \in R^{n_x \times n_y}$, where k denotes the compressed frame number in a single image, n_x and n_y denote the spatial size of the fluorescent dynamics in the x and y directions. Thus, the measured image can be expressed by

$$Y = \sum_{i=1}^{k} X_i \odot C_i + N, \tag{1}$$

where $\odot$ denotes the element-wise product, and $N \in R^{n_x \times n_y}$denotes the noise during the image measurement. For simplification, the process can be further written by vectorized form as

$$\boldsymbol{y} = A\boldsymbol{x} + \boldsymbol{n}, \tag{2}$$

where $\boldsymbol{y}$, $\boldsymbol{x}$ and $\boldsymbol{n}$ are, respectively, the vectorized Y, X and N, and A is the whole compressed measurement operation. Then, $\boldsymbol{x}$ needs to be solved according to the measurement $\boldsymbol{y}$ and compressed measurement operation A with the help of image reconstruction algorithm. Since Eq. (2) is an ill-posed problem, it can be solved by transferring it into an optimization problem and is given by

$$\hat{\boldsymbol{x}} = \arg\min \frac{1}{2}\|\boldsymbol{y} - A\boldsymbol{x}\|_2^2 + \lambda\Phi(\boldsymbol{x}), \tag{3}$$

where $\hat{\boldsymbol{x}}$ denotes the estimation solution of the problem, $||.||_2$ denotes L_2 norm, λ is the regularization parameter, and Φ is the regularization function. To utilize the Plug-and-Play (PnP) framework with different sparse constraints or priors, one can change the optimization problem into the following format by an alternating direction method of multipliers (ADMM) [27–29], which is written as

$$(\hat{\boldsymbol{x}}, \hat{v}) = \arg\min_{x,v} \frac{1}{2}||\boldsymbol{y} - A\boldsymbol{x}||_2^2 + \lambda\,\Phi(\boldsymbol{v}),\ subject\ to\ \boldsymbol{x} = \boldsymbol{v}. \tag{4}$$

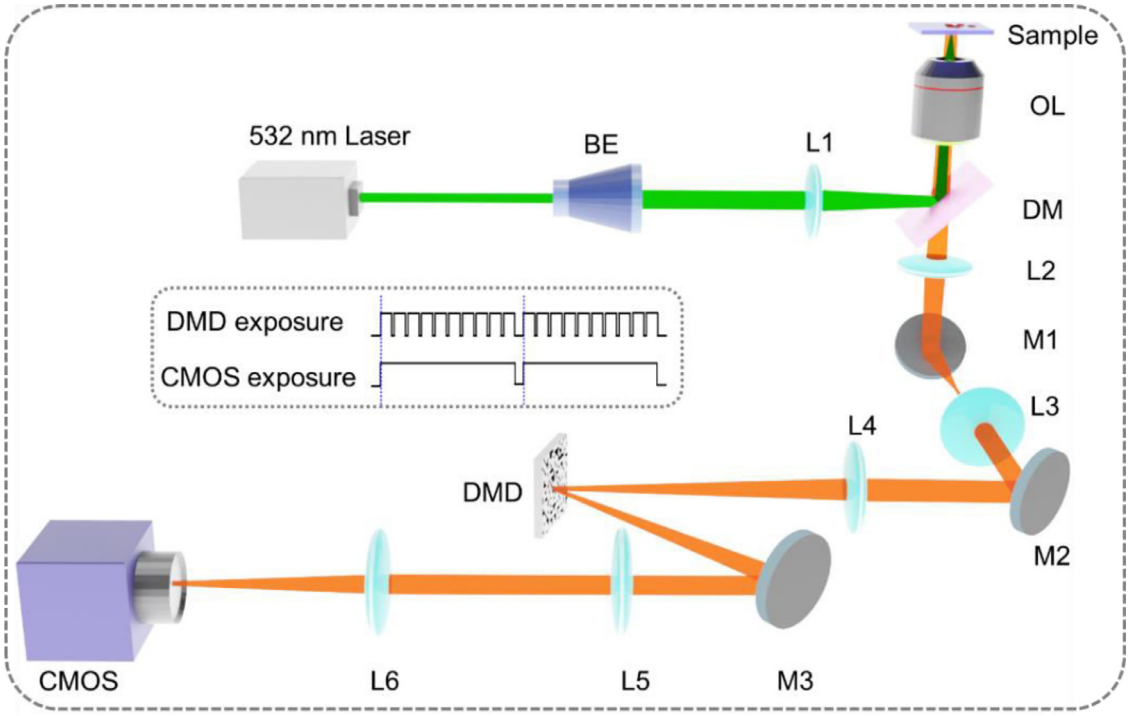

Fig. 1. Experimental arrangement of high-speed CWFM. BE: beam expander; L1–6: Lens; DM: dichroic mirror; OL: objective lens; M1–3: mirror; DMD: digital micromirror device.

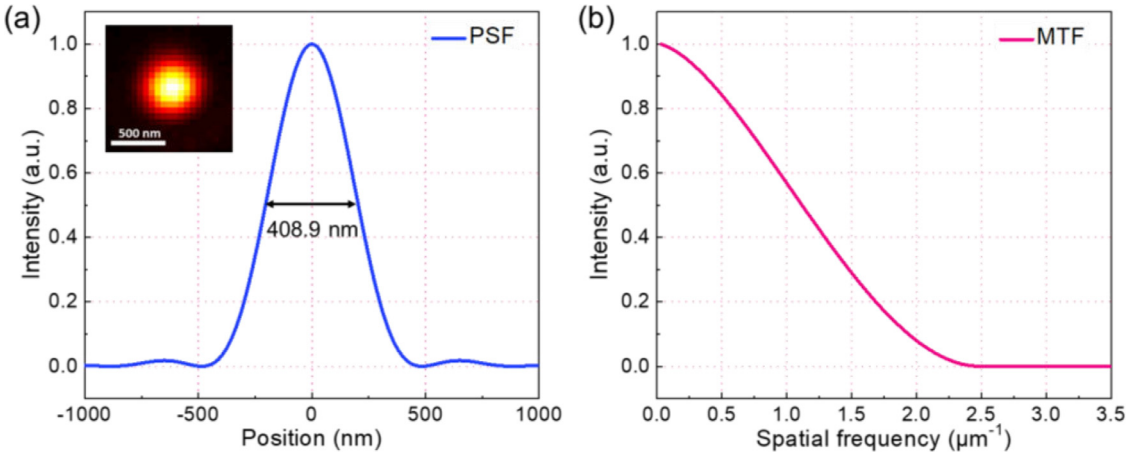

Fig. 2. Point spread function (a) and modulation transfer function (b) of our CWFM system. The inset shows the measured image of a 50 nm fluorescent bead with the CWFM system.

In Eq. (4), this optimization problem can be further divided into the following sub-problems and is given by

$$\boldsymbol{x}^{(k+1)} = \arg\min_{\boldsymbol{x}} \frac{1}{2}\|\boldsymbol{y} - A\boldsymbol{x}\|_2^2 + \frac{\rho}{2}\left\|\boldsymbol{x} - \left(\boldsymbol{v}^{(k)} - \frac{1}{\rho}\boldsymbol{u}^{(k)}\right)\right\|_2^2, \tag{5}$$

$$\boldsymbol{v}^{(k+1)} = \arg\min_{\boldsymbol{v}} \lambda\Phi(\boldsymbol{v}) + \frac{\rho}{2}\left\|\boldsymbol{v} - \left(\boldsymbol{x}^{(k)} + \frac{1}{\rho}\boldsymbol{u}^{(k)}\right)\right\|_2^2, \tag{6}$$

$$\boldsymbol{u}^{(k+1)} = u^{(k)} + \rho\left(\boldsymbol{x}^{(k+1)} - \boldsymbol{v}^{(k+1)}\right), \tag{7}$$

where $\boldsymbol{v}$ and $\boldsymbol{u}$ are auxiliary intermediate variables of ADMM, ρ is a scale factor of ADMM. Eq. (6) can be solved by an off-the-shelf denoiser D with the sparse constraints or priors and is written as

$$\boldsymbol{v}^{(k+1)} = D\left(\boldsymbol{x}^{(k)} + \frac{1}{\rho}\boldsymbol{u}^{(k)}\right). \tag{8}$$

In our image reconstruction, the video with compressed frames is first initialized into video with multi-fold subframes, here the subframe number depends on the temporal compressive rate, and then it is iteratively optimized using ADMM frameworks with alternate FFDnet and FastDVDnet priors, as shown in Fig. 3(a). The iteration runs in the groups with number of n, and every group sequentially contains FFDnet and FastDVDnet priors with number of m. FFDnet is able to handle a wide range of noise levels and remove spatially variant noise with a tunable noise level map as the input and downsample operation. A cascaded convolution neural network (CNN) is utilized to process subframes. The architecture of FFDnet is shown in Fig. 3(b). Besides, FastDVDnet is introduced to maintain the temporal continuity during the video reconstruction. FastDVDnet is consist of two denoising steps, and the blocks in these steps are all built with U-net framework, as shown in Fig. 3(c). Three adjacent frames are used as the input of a block, and every output frame is derived from five adjacent in-

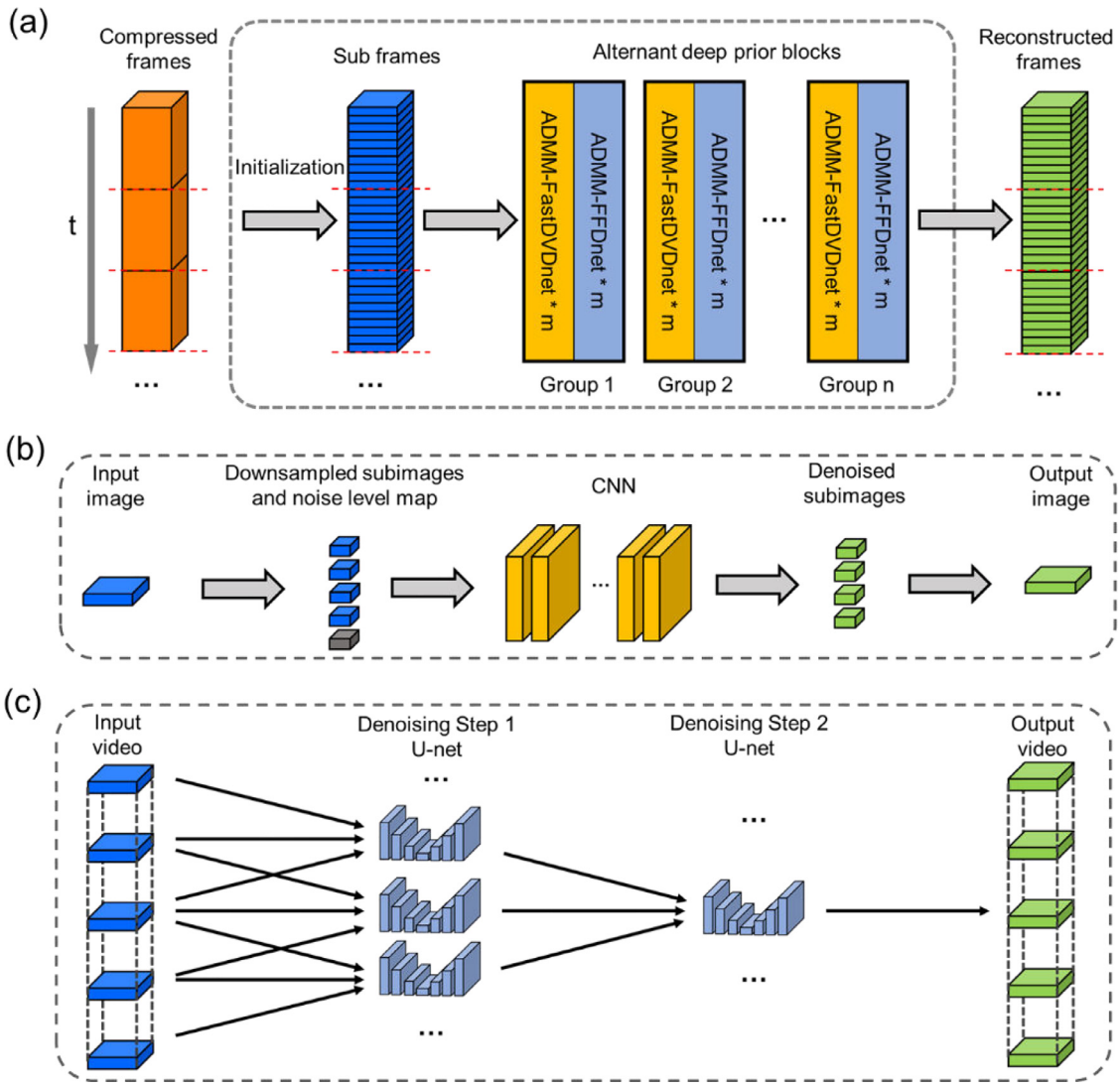

Fig. 3. Image reconstruction algorithm of high-speed CWFM. The whole framework of image reconstruction with alternate FFDnet and FastDVDnet priors (a), together with the architecture of FFDnet (b) and FastDVDnet (c).

put images, thus the temporal continuity can be implicitly employed. Sometimes, the weird artifacts appear in the images reconstructed by FFDnet, especially for those images with low SNR. The issue will seriously affect the reliability of FFDnet. Considering the temporal continuity between adjacent frames, the weird artifacts of single image can be removed, since it normally doesn't behave the similarity in adjacent frames. With the alternate manner of our image reconstruction algorithm, both the powerful denoising ability of FFDnet and the temporal continuity maintaining of FastDVDnet are utilized, thus high-speed video with high-quality images can be achieved. It should be pointed out that, since the video is integrally processed, the temporal continuity of the subframes not only from the same compressed frame but also from adjacent compressed frame is utilized in our image reconstruction algorithm.

3. Results and discussion

Firstly, the high-speed imaging ability of our CWFM system is verified, a simple and common experiment is performed by measuring the moving fluorescent beads. Here, the polystyrene fluorescent beads with the diameter of 500 nm are dispersed on a slide, and the slide is mounted on a sample stage that is evenly moved in the horizontal direction. The frame rate of the camera is 200 Hz, and the refresh rate of the DMD is set as 2000 Hz, thus the temporal compressive rate is 10. In this experiment, the objective lens is Olympus PLCN60 × 0.8 NA, and a 2 × barlow lens is also utilized to increase the magnification of the fluorescence image. A server with Intel i9–12900KF, 64 GB of RAM and NVIDIA GeForce RTX3090 is utilized to process the experimental images, and the computation time is about 120 s for every compressed image. A video with compressed frames is captured with our high-speed CWFM system under the 532 nm laser excitation, and one selected frame of the measured video is shown in Fig. 4(a). As can be seen, only two fluorescence bars are captured in this image, which are attributed to the moving blur of the two fluorescent beads. Meanwhile, one of the coding patterns applied on the DMD is also given in Fig. 4(b). Ten images reconstructed by our algorithm with the alternate deep priors are shown in Fig. 4(c), associated with the extracted moving traces of the two fluorescent beads, the trace is calculated by a centroid method [30]. Obviously, the ten images with clear spatial structure can be reconstructed from the compressed image in Fig. 4(a), and therefore the imaging speed is increased by an order of magnitude. Additionally, the moving speed of the two fluorescent beads can be calculated to be about 1.3 mm/s based on the experimental measurement in Fig. 4(c), which is the same as that of the sample stage. The moving speed of fluorescent beads can be measured by our CWFM system with single exposure, which is very useful for the detection of unrepeatable or irreversible dynamics. The

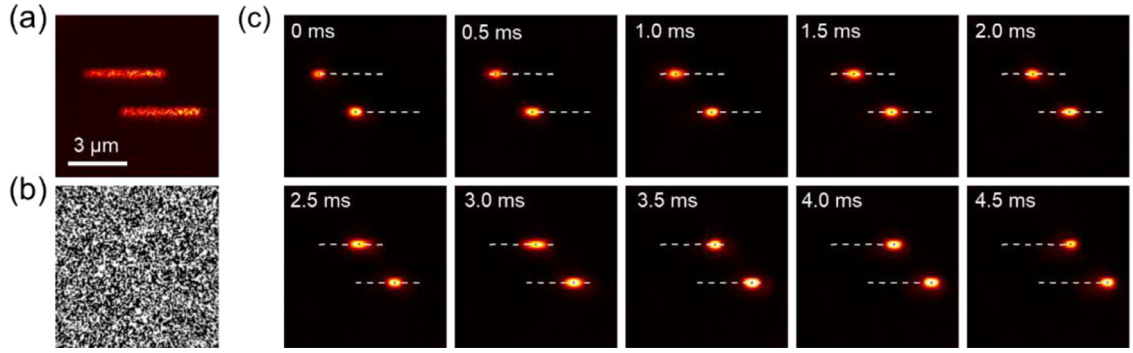

Fig. 4. Imaging the movement of fluorescent beads on a slide by high-speed CWFM. (a) One of compressed images; (b) One of spatial coding pattern; (c) Reconstructed images from Fig. 4(a).

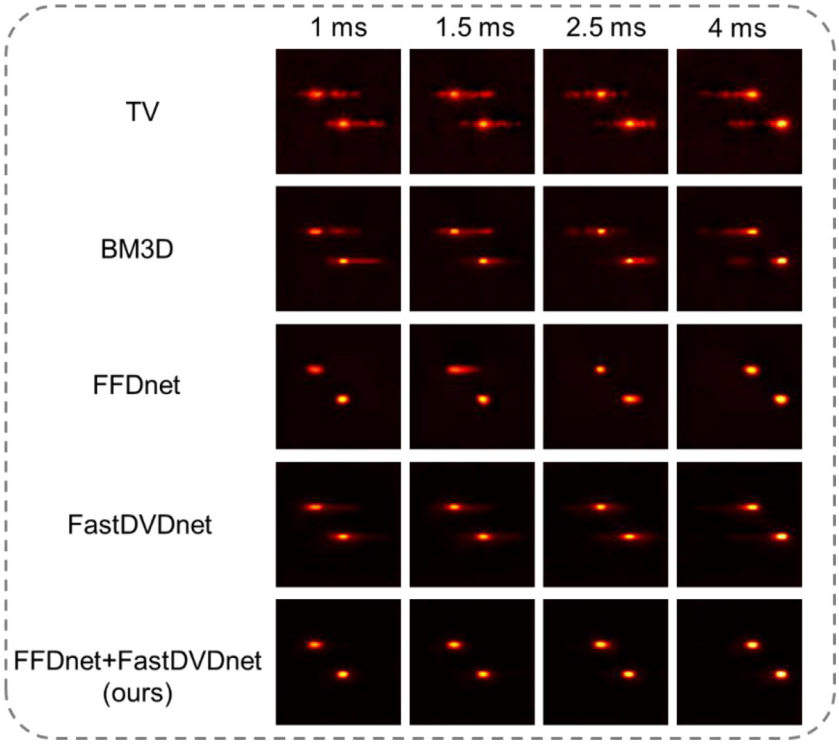

Fig. 5. Reconstructed images by the reconstruction algorithms with TV, BM3D, FFDnet, FastDVDnet and our FFDnet+FastDVDnet priors.

whole video of the moving fluorescent beads on the slide is provided in **Visualization 1**.

To demonstrate the superiority of our algorithm with the alternate deep denoisers, the image reconstructions with some common priors are also conducted, including TV, BM3D, FFDnet, and FastDVDnet. Four out of ten frames are selected, as shown in Fig. 5. All the images reconstructed with the TV prior shows obvious artifacts, which is due to that the TV prior can't provide enough constrain during the image reconstruction for the high noise level under the short exposure time. Similarly, the images reconstructed with the BM3D prior also show the same behavior with the obvious artifacts. The measured dynamic scene for the movement of fluorescent beads is relatively simple, and the non-local similarity between the blocks of these images is quite low, thus BM3D doesn't perform as well as the denoising of the image with complex details. As for the images reconstructed with the FFDnet prior, the artifacts are greatly eliminated, and the spatial profile of fluorescent beads in some frames can be clearly distinguished, while there are still obvious residual artifacts in some frames. Obviously, FFDnet can only provide good constrain for some frames, which is because the noise level and intensity weight in these frames are different and FFDnet is to individually denoise these frames, thus the effect of image reconstruction is different in these frames. In contrast, FastDVDnet can well suppress the flickers between adjacent frames by taking advantage of their temporal continuity. As can be seen, these images reconstructed with the FastDVDnet prior shows good temporal continuity, but the ability to remove the artifacts is weaker than the FFDnet prior. However, our algorithm, which alternatively utilizes the FFDnet and FastDVDnet priors, shows the better performance in both removing the artifacts and maintaining the temporal continuity, therefore it is highly desirable for the image reconstruction in high-speed CWFM.

Given the outstanding imaging speed and remarkable image quality, high-speed CWFM can be applied to capture the dynamics in various areas. We further study the hydrodynamics by detecting the flow of fluorescent beads in the water across a corner of microchannel with high-speed CWFM. The fluorescent beads with the diameter of 3 μm are dispersed into the water, and then are sent into a microflow chip (MesoBioSystem, PIE-13–001) by an injection pump (MesoBioSystem, MS101P). The flux of the water is set as 3 μl/min. The bright field microscopy image of this microflow chip under the white light illumination with the 5 × objective lens is first recorded, as shown in Fig. 6(a), and the width of the narrowest section in the microchannel is determined to be about 70 μm. Then, the microflow chip is located on the sample stage

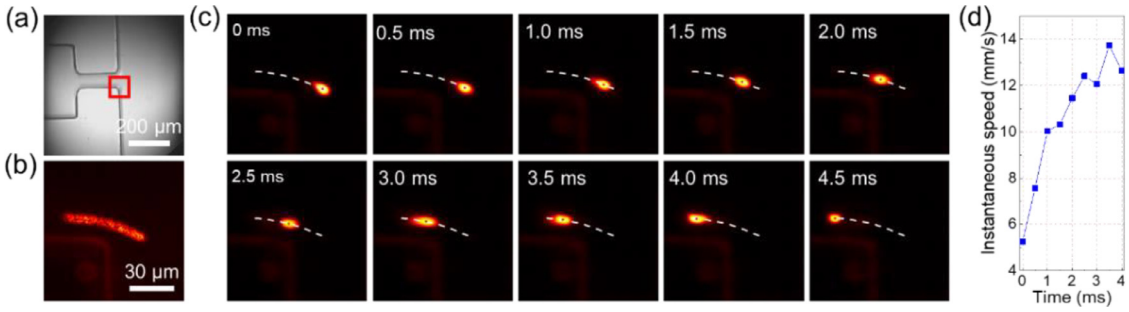

Fig. 6. Imaging the flow of a fluorescent bead in the water across a corner in microchannel by high-speed CWFM. (a) Image of microflow chip under white light illumination; (b) One of compressed image; (c) Reconstructed images from Fig. 6(b); (d) Extracted instantaneous speed from Fig. 6(c).

of high-speed CWFM with the 20 × objective lens. The dynamic scene that a fluorescent bead flows across the corner of microchannel under the 532 nm laser excitation is recorded with a CMOS camera of 200 Hz, and the temporal compressive rate is also 10, which is the same as the experiment in Fig. 4. Since the flowing speed of the water is quite high, only the blurred images can be directly captured by the camera, and one frame of the recorded video is selected to be shown in Fig. 6(b). The captured compressed video is processed with our algorithm embedded with the alternate deep priors. Thus, a high-speed video with the frame rate of 2000 Hz is recovered. Here, only ten reconstructed frames that are corresponding to the compressed frame in Fig. 6(b) are shown in Fig. 6(c), associated with the flowing trace. According to the reconstructed data, the radius of the trajectory is determined as about 0.11 mm, and the flow of the fluorescent bead shows a process of accelerating first and then keeping at a uniform speed, as shown in Fig. 6(d), here the instantaneous speed is calculated by extracting the moving distance of the fluorescent bead between adjacent frames. The final flowing speed of the fluorescent bead is estimated to be about 12.6 mm/s, which is almost the same as the flowing speed of the water in the narrowest section with 12.9 mm/s calculated based on the flux and microchannel diameter. This observation is consistent with the law of hydrodynamics, the water flow will be accelerated at the corner of microchannel from wide to narrow sections. The video of the fluorescent bead across a corner of microchannel is provided in **Visualization 2**.

However, there still exist some shortcomings in high-speed CWFM. For example, the spatial shape of the fluorescent beads in the reconstructed images is an ellipse instead of a circle. This is mainly due to the fact that the movement of fluorescent beads is continuous, while the spatial coding and image acquirement are temporally discrete. When the moving speed of the target is high enough, every frame of the captured video is an integration of a short dynamic scene. Thus, the deformation is inevitable for imaging the fast-moving target. To alleviate this effect, a higher imaging speed is required. The SNR is relatively low at high imaging speed, but the high-quality images with the frame rate of 2000 Hz can still be obtained in our CWFM system. Limited by the photo-bleaching and photo-damage, the fluorescence signal can't be enhanced by simply increasing the illumination source power. A complementary coding strategy [31,32] can be utilized to increase the SNR for the higher imaging speed and the better image quality. As for the algorithm, the model-based priors can also cooperate with the deep priors, such as TV denoiser and deep image priors [16], WNNM denoiser and FFDnet [29], TV denoiser and FFDNet [33]. Furthermore, the combined mode of the two different priors is not limited in the alternation during the iteration, and the weight balance [34] or self-attention mechanism [35] can also be utilized.

4. Conclusions

In summary, we have developed a high-speed CWFM with an alternant deep denoisers-based image reconstruction algorithm to break the imaging speed limitation of conventional WFM by introducing a coded aperture temporal compressive imaging method. In our image reconstruction, an algorithm with alternate deep priors is specially designed to resolve the inevitable problem of low SNR in the fluorescence imaging under high frame rate. Using the powerful denoising ability of FFDnet and the temporal correlation maintaining of FastDVDnet, our algorithm showed a great image reconstruction capability in both spatial and temporal dimensions by removing the artifacts and suppressing the flickers between adjacent frames. In our CWFM system, the imaging speed can be up to 2000 Hz by using an ordinary CMOS camera of 200 Hz, which is increased by an order of magnitude. The excellent performance of our CWFM system in the high-speed imaging was experimentally verified by measuring the movement of fluorescent beads on a slide. Using our high-speed CWFM system, the hydrodynamics was experimentally observed by measuring the flow of a fluorescent bead in the water across the corner of microchannel. Our high-speed CWFM technique provides a well-established tool for imaging or tracking the kinetic fluorescent target, such as flowing imaging [36], cell tracking [37], and so on, which will definitely promote the rapid development of related areas. In addition, the system configuration and reconstruction algorithm of high-speed CWFM can be further extended to other fluorescence-based wide-field microscopy towards a higher imaging speed through proper modification, such as light sheet fluorescence microscopy [38], wide-field fluorescence lifetime microscopy [39], and structured illumination super-resolution microscopy [40].

Declaration of Competing Interest

The authors declare that they have no known competing financial interests or personal relationships that could have appeared to influence the work reported in this paper.

CRediT authorship contribution statement

Yilin He: Conceptualization, Methodology, Software. **Yunhua Yao:** Conceptualization, Methodology, Formal analysis, Writing – original draft. **Yu He:** Investigation, Visualization, Validation. **Zhengqi Huang:** Investigation. **Pengpeng Ding:** Data curation. **Dalong Qi:** Formal analysis, Funding acquisition. **Zhiyong Wang:** Formal analysis. **Tianqing Jia:** Formal analysis. **Zhenrong Sun:** Supervision, Resources. **Shian Zhang:** Supervision, Project administration, Writing – review & editing, Funding acquisition.

Data availability

Data will be made available on request.

Acknowledgments

This work was partly supported by National Natural Science Foundation of China (91850202, 92150301, 12074121, 62105101, 62175066,

11727810, 12034008, 12274129, 12274139); Science and Technology Commission of Shanghai Municipality (21XD1400900, 20ZR1417100, 21JM0010700).

Supplementary materials

Supplementary material associated with this article can be found, in the online version, at doi:10.1016/j.optlaseng.2023.107541.

References

[1] Lichtman JW, Conchello J. Fluorescence microscopy. Nat Methods 2005;2:910–19.
[2] Yuste R. Fluorescence microscopy today. Nat Methods 2005;2:902–4.
[3] Axelrod D. Total internal reflection fluorescence microscopy. In: Methods in cell biology. Elsevier; 1989. p. 245–70.
[4] Gong H, Xu D, Yuan J, Li X, Guo C, Peng J, Li Y, Schwarz LA, Li A, Hu B. High--throughput dual-colour precision imaging for brain-wide connectome with cytoarchitectonic landmarks at the cellular level. Nat Commun 2016;7:1–12.
[5] Ablasser A, Schmid-Burgk JL, Hemmerling I, Horvath GL, Schmidt T, Latz E, Hornung V. Cell intrinsic immunity spreads to bystander cells via the intercellular transfer of cGAMP. Nature 2013;503:530–4.
[6] Irvine DJ, Purbhoo MA, Krogsgaard M, Davis MM. Direct observation of ligand recognition by T cells. Nature 2002;419:845–9.
[7] Pavlova I, Williams M, El-Naggar A, Richards-Kortum R, Gillenwater A. Understanding the biological basis of autofluorescence imaging for oral cancer detection: high-resolution fluorescence microscopy in viable tissue. Clin Cancer Res 2008;14:2396–404.
[8] Ghaznavi F, Evans A, Madabhushi A, Feldman M. Digital imaging in pathology: whole-slide imaging and beyond. Annu Rev Pathol Mech 2013;8:331–59.
[9] Gelderblom EC. Ultra-high-speed fluorescence imaging, Enschede: Universiteit Twente; 2012. PhD Thesis.
[10] Sugii Y, Okuda R, Okamoto K, Madarame H. Velocity measurement of both red blood cells and plasma of *in vitro* blood flow using high-speed micro PIV technique. Meas Sci Technol 2005;16:1126.
[11] Calisesi G, Ghezzi A, Ancora D, D'Andrea C, Valentini G, Farina A, Bassi A. Compressed sensing in fluorescence microscopy. Prog Biophys Mol Bio 2022;168:66–80.
[12] Studer V, Bobin J, Chahid M, Mousavi HS, Candes E, Dahan M. Compressive fluorescence microscopy for biological and hyperspectral imaging. Proc Natl Acad Sci USA 2012;109:E1679–87.
[13] Pascucci M, Ganesan S, Tripathi A, Katz O, Emiliani V, Guillon M. Compressive three-dimensional super-resolution microscopy with speckle-saturated fluorescence excitation. Nat Commun 2019;10:1–8.
[14] Liu Y, Suo J, Zhang Y, Dai Q. Single-pixel phase and fluorescence microscope. Opt Express 2018;26:32451–62.
[15] Yuan X, Pang S. Structured illumination temporal compressive microscopy. Biomed Opt Express 2016;7:746–58.
[16] Qiao M, Liu X, Yuan X. Snapshot temporal compressive microscopy using an iterative algorithm with untrained neural networks. Opt Lett 2021;46:1888–91.
[17] Yuan X, Brady DJ, Katsaggelos AK. Snapshot compressive imaging: theory, algorithms, and applications. IEEE Signal Proc Mag 2021;38:65–88.
[18] Llull P, Liao X, Yuan X, Yang J, Kittle D, Carin L, Sapiro G, Brady DJ. Coded aperture compressive temporal imaging. Opt Express 2013;21:10526–45.
[19] Yuan X. Generalized alternating projection based total variation minimization for compressive sensing. In: Proceedings of the IEEE international conference on image processing. IEEE; 2016. p. 2539–43.
[20] Maggioni M, Boracchi G, Foi A, Egiazarian K. Video denoising, deblocking, and enhancement through separable 4-D nonlocal spatiotemporal transforms. IEEE Trans Image Process 2012;21:3952–66.
[21] Yang J, Yuan X, Liao X, Llull P, Brady DJ, Sapiro G, Carin L. Video compressive sensing using Gaussian mixture models. IEEE Trans Image Process 2014;23:4863–78.
[22] Liu Y, Yuan X, Suo J, Brady DJ, Dai Q. Rank minimization for snapshot compressive imaging. IEEE Trans Pattern Anal 2018;41:2990–3006.
[23] Zhang K, Zuo W, Chen Y, Meng D, Zhang L. Beyond a gaussian denoiser: residual learning of deep CNN for image denoising. IEEE Trans Image Process 2017;26:3142–55.
[24] Zhang K, Zuo W, Zhang L. FFDNet: toward a fast and flexible solution for CNN-based image denoising. IEEE Trans Image Process 2018;27:4608–22.
[25] Tassano M, Delon J, Veit T. Fastdvdnet: towards real-time deep video denoising without flow estimation. In: Proceedings of the IEEE/CVF conference on computer vision and pattern recognition. IEEE/CVF; 2020. p. 1354–63.
[26] Theer P, Mongis C, Knop M. PSFj: know your fluorescence microscope. Nat Methods 2014;11:981–2.
[27] Boyd S, Parikh N, Chu E, Peleato B, Eckstein J. Distributed optimization and statistical learning via the alternating direction method of multipliers. Foundations and Trends in Machine Learning 2010;3:1–112.
[28] Chan SH, Wang X, Elgendy OA. Plug-and-play ADMM for image restoration: fixed–point convergence and applications. IEEE Trans Comput Imaging 2016;3:84–98.
[29] Yuan X, Liu Y, Suo J, Dai Q. Plug-and-play algorithms for large-scale snapshot compressive imaging. In: Proceedings of the IEEE/CVF conference on computer vision and pattern recognition. IEEE/CVF; 2020. p. 1447–57.
[30] Nascimento JC, Abrantes AJ, Marques JS. An algorithm for centroid-based tracking of moving objects. In: Proceedings of the IEEE international conference on acoustics, speech, and signal processing. IEEE; 1999. p. 3305–8.
[31] Wang L, Gao D, Shi G, Niu Y. Double-channel compressive spectral imaging via complementary code patterns. In: Proceedings of the IEEE international conference on signal processing, communication and computing. IEEE; 2013. p. 1–5.
[32] Ma Y, Lee Y, Best-Popescu C, Gao L. High-speed compressed-sensing fluorescence lifetime imaging microscopy of live cells. Proc Natl Acad Sci USA 2021;118:e2004176118.
[33] Qiu H, Wang Y, Meng D. Effective snapshot compressive-spectral imaging via deep denoising and total variation priors. In: Proceedings of the IEEE/CVF conference on computer vision and pattern recognition. IEEE/CVF; 2021. p. 9127–36.
[34] Zhang Z, Xu C, Yang J, Tai Y, Chen L. Deep hierarchical guidance and regularization learning for end-to-end depth estimation. Pattern Recognit 2018;83:430–42.
[35] Zhao H, Jia J, Koltun V. Exploring self-attention for image recognition. In: Proceedings of the IEEE/CVF conference on computer vision and pattern recognition. IEEE/CVF; 2020. p. 10076–85.
[36] Mikami H, Kawaguchi M, Huang C, Matsumura H, Sugimura T, Huang K, Lei C, Ueno S, Miura T, Ito T. Virtual-freezing fluorescence imaging flow cytometry. Nat Commun 2020;11:1–11.
[37] Sutton EJ, Henning TD, Pichler BJ, Bremer C, Daldrup-Link HE. Cell tracking with optical imaging. Eur Radiol 2008;18:2021–32.
[38] Stelzer EH. Light-sheet fluorescence microscopy for quantitative biology. Nat Methods 2015;12:23–6.
[39] Bowman AJ, Klopfer BB, Juffmann T, Kasevich MA. Electro-optic imaging enables efficient wide-field fluorescence lifetime microscopy. Nat Commun 2019;10:1–8.
[40] Gustafsson MG. Surpassing the lateral resolution limit by a factor of two using structured illumination microscopy. J Microsc 2000;198:82–7.